Garrido, L., Pozuelo, J., López-González, M., Yan. G., Fang, J. & Riande, E. (2012): Influence of the Water Content on the Diffusion Coefficients of Li+ and Water across Naphthalenic Based Copolyimide Cation-Exchange Membranes. The Journal of Physical Chemistry B, 116 (38), pp.:11754-11766.

DOI: 10.1021/jp30653220

Influence of the Water Content on the Diffusion Coefficients of Li^+ and Water across Naphthalenic Based Copolyimide Cation-Exchange Membranes

Leoncio Garrido,[†] Javier Pozuelo,[‡] Mar López-González,[†] Gengwei Yan,[§] Jianhua Fang,*[,§] and Evaristo Riande*[,†]

[†] Departamento de Química Física, Instituto de Ciencia y Tecnología de Polímeros, Consejo Superior de Investigaciones Científicas (ICTP-CSIC), 28006 Madrid, Spain

[‡] Departamento de Ciencia e Ingeniería de Materiales e Ingeniería Química (IAAB), Universidad Carlos III de Madrid, 28911 Leganés, Spain

§ School of Chemistry and Chemical Engineering, Shanghai Jiao Tong University, Shanghai 200240, China

ABSTRACT

The transport of lithium ions in cation-exchange membranes based on sulfonated copolyimide membranes is reported. Diffusion coefficients of lithium are estimated as a function of the water content in membranes by using pulsed field gradient (PFG) NMR and electrical conductivity techniques. It is found that the lithium transport slightly decreases with the diminution of water for membranes with water content lying in the range $14 < \lambda < 26.5$, where λ is the number of molecules of water per fixed sulfonate group. For $\lambda < 14$, the value of the diffusion coefficient of lithium experiences a sharp decay with the reduction of water in the membranes. The dependence of the diffusion of lithium on the humidity of the membranes calculated from conductivity data using Nernst−Planck type equations follows a trend similar to that observed by NMR. The possible explanation of the fact that the Haven ratio is higher than the unit is discussed. The diffusion of water estimated by ^{1}H PFG-NMR in membranes neutralized with lithium decreases as λ decreases, but the drop is sharper in the region where the decrease of the diffusion of protons of water also undergoes considerable reduction. The diffusion of lithium ions computed by full molecular dynamics is similar to that estimated by NMR. However, for membranes with medium and low concentration of water, steady state conditions are not reached in the computations and the diffusion coefficients obtained by MD simulation techniques are overestimated. The curves depicting the variation of the diffusion coefficient of water estimated by NMR and full dynamics follow parallel trends, though the values of the diffusion coefficient in the latter case are somewhat higher. The WAXS diffractograms of fully hydrated membranes exhibit the ionomer peak at q = 2.8 nm−1, the peak being shifted to higher q as the water content of the membranes decreases. The diffractograms present additional peaks at higher q, common to wet and dry membranes, but the peaks are better resolved in the wet membranes. The ionomer peak is not detected in the diffractograms of dry membranes.

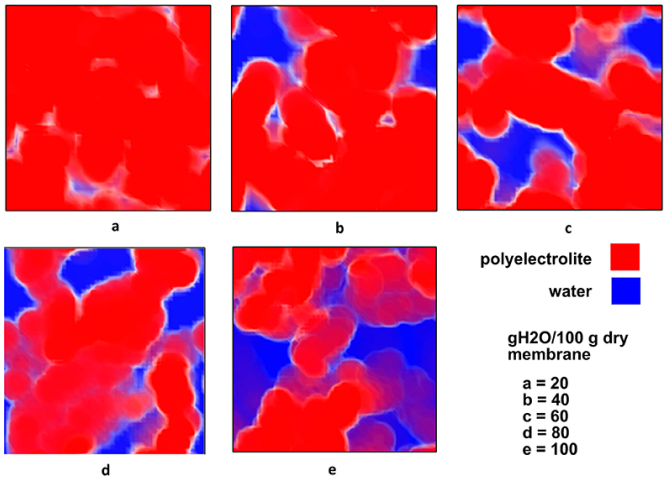

INTRODUCTION

Since ions are much heavier than electrons, their motion in disordered systems is far less governed by quantum mechanics in such a way that for vibrations below 100 MHz motion takes place by activated hopping between holes that act as charge compensating sites. The potential energy landscape through which ion motion occurs contains a wide distribution of depths and barriers resulting from different binding energies at residence sites and different saddle energies between residence sites as well as interactions between the ions.[1] As a result, the larger the time scale, the wider is the configurational space explored by the ions. Although the motion of ion charge carriers is reflected in experimental measurements such as the conductivity, a theory describing motions of ions in disordered systems has not yet been elaborated.[2]

In general, the *ac* electrical response of disordered systems involves the superposition of different contributions: (a) dielectric response of the bound charges (dipolar response), (b) hopping of localized charge carriers, and (c) response produced by deformation of the molecular structure following the diffusion of charges though percolation paths.[3] In this context, the isotherms describing the real component, σ', of the complex conductivity, σ^*, of disordered ion conducting systems in the frequency domain is independent of frequency in the low frequency region, reflecting dc conductivity caused by ion transport in the samples.[4] However, at a given frequency ω_c, σ'

Scheme 1. Synthesis of 4,4′-Bis(4-aminophenoxy)biphenyl (BAPB)

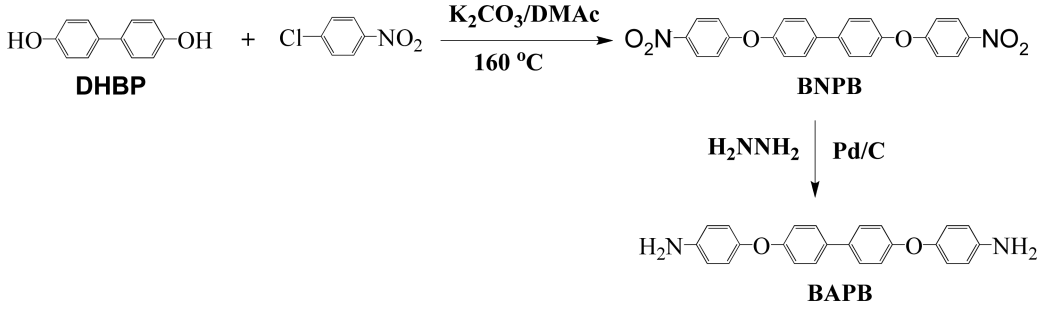

departs from the plateau and starts to increase with increasing frequency as a result of dispersive dipolar processes taking place in the system and therefore ω_c can be viewed as the onset of the ac conductivity. Polar polymers with nanodomains formed by segregation of polar side groups from the nonpolar backbone[5,6] present just above ω_c a distributed Maxwell–Wagner–Sillars (MWS) relaxation produced by relatively long distance charges transport. In increasing order of frequency, the glass–rubber relaxation arising from segmental motions of the polymer chains as well as secondary relaxation processes produced by local motions affect the ac conductivity of polymeric systems. Similar behavior is exhibited by other polar polymers, though MWS charges transport seems to be restricted to heterogeneous systems. At very high frequencies, the ac conductivity approaches a regime $\sigma'(\omega) \cong A\omega^n$, where A is only weakly temperature dependent and n is a fractional exponent less than 1.[7] This nearly constant loss regime appears in many systems including not only polymers but also glassy, crystalline, and molten ion conductors, independently of specific chemical and physical structures.[7,8]

Anions and cations anchored respectively to macromolecular chains in cation- and anion-exchange membranes are tightly joined by electrical forces to their respective mobile counterions in the case of dry membranes, in such a way that the motions of the latter ions are severely restricted. The ac conductivity of dry ion-exchange membranes displays some of the features of polar polymers. However, the presence of water changes drastically the situation in such a way that at high frequencies the real component of the complex conductivity is frequency independent. Counterions in wet ion-exchange membranes act as charge carriers, and these systems may exhibit relatively high dc conductivity. Water intervenes in the dissociation of the fixed ionic groups, screening the counterions from the fixed ionic groups anchored to the polymer structure, and it is the medium through which counterions diffuse. It is found experimentally that the dc conductivity of ion-exchange membranes with very low water content is very small as a consequence of the fact that the ionic groups anchored to the chains of the membranes are not dissociated. Theoretical calculations predict that the formation of hydronium groups that act as carriers in the conductive process of acidic membranes requires at least two molecules of water per sulfonic acid group.[9] Recent experimental work suggests that the solvation process of Nafion membranes involves four molecules of water per sulfonic acid group.[10] Owing to the fact that the presence of water decreases the friction of the mobile counterions with the surroundings, the ohmic conductivity decreases as the water content of the membranes increases.

Counterion diffusion in ion-exchange membranes can be estimated from the electrical ohmic conductivity of these systems. In addition to conductivity, pulsed field gradient (PFG) NMR can be used to calculate the diffusion coefficients of proton in acidic cation-exchange membranes.[11−17] However, the values of the diffusion coefficients obtained by conductivity and NMR techniques may differ due to the complex mechanisms involved in the carrier transport. For example, proton transport in fully hydrated high conductivity acidic membranes is described at the molecular level by a hopping mechanism or Grotthuss transport. For low conductivity membranes, a vehicular type mechanism through water acting as a carrier describes the proton transport better.[9,18,19] Proton diffusion in high conductivity hydrated acidic membranes determined by ^{1}H PFG-NMR is lower than that estimated by electrical conductivity.[11,16] The cause of this discrepancy lies in that the diffusion coefficient obtained by the former technique is the average of the diffusion coefficients of the fast acid protons and the slow protons of water. As the water content in the membranes decreases, the ratio between the proton mobility coefficients obtained by the two techniques comes close to the unit. In this case, the conductive mechanism is of vehicular type. In most conducting solids, the Haven ratio H_R, i.e., the ratio of the tracer diffusion coefficient (D^*) to the diffusion coefficient of the charge carrier, D_σ, obtained from the conductivity using Nernst–Planck type equations, is lower or equal to the unit.[1]

Owing to the fact that the ^{1}H PFG-NMR technique impedes to obtain directly the diffusion of protons, the electrical carriers in acidic membranes, it is desirable to use this technique in the study of charge transport in membranes where the couterions are well-defined probes, such as lithium. There is a wealth of information concerning the conductivity of lithium cations in neutral polymers, such as poly(ethylene oxide) and other polymers,[20−23] but relatively little work has been focused on the study of lithium transport in cation exchange membranes in the lithium form. Most of the research carried out in this regard is centered on perfluorinated type membranes such as Nafion.[24−26] It is important to extend these studies to other types of cation-exchange membranes based on polymers with high thermal and chemical stability, such as poly(aryletherketone)s, polysulfones, polynaphthalenic polyimides, etc. Owing to the rigidity of the molecular chains of these polymers, the segregation of hydrophilic moieties from hydrophobic ones to form percolation paths for counterion transport is severely hindered.[27] As a result, only membranes based on rigid polyelectrolytes with high ion-exchange capacity may exhibit dc conductivity comparable to that of Nafion.

This work reports a comparative study of the diffusion of lithium cations in sulfonated naphthalenic polyimide (SNCPI) membranes as measured by spin–echo ^{7}Li PFG-NMR and electrical conductivity. In addition, the diffusion coefficient of

Scheme 2. Synthesis of the Sulfonated Polyimide (SNCPI)

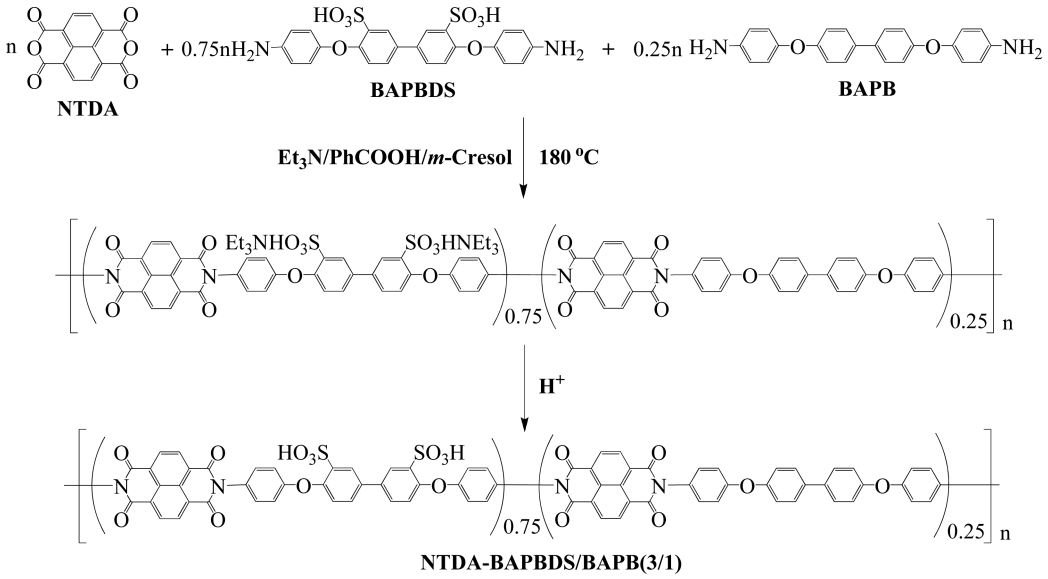

water in the membranes is measured as a function of the water content using the ^{1}H PFG-NMR technique. Attention is paid to the segregation of hydrophilic moieties from hydrophobic ones reflected in X-ray diffractograms of the membranes. The structure of water, as well the diffusion of the lithium ion and water in membranes with different water content, are studied by full molecular dynamics.

EXPERIMENTAL SECTION

Materials. 1,4,5,8-Naphthalenetetracarboxylic dianhydride (NTDA) was purchased from Beijing Multi Technology Co., Ltd., China. 4,4′-Dihydroxybiphenyl (DHBP) was purchased from TCI. *N*,*N*-dimethylacetamide (DMAc), triethylamine (Et_3N), *m*-cresol, benzoic acid, toluene, and potassium carbonate were purchased from Sinopharm Chemical Reagent Co., Ltd. (SCRC). NTDA was dried at 160 °C in a vacuum for 20 h before use. Et_3N was distilled and dried with a 4 Å molecular sieve prior to use. Other reagents were used as received. The nonsulfonated diamine, 4,4′-bis(4-aminophenoxy)biphenyl (BAPB), was synthesized by two-step reactions (Scheme 1), and the experimental details are described as follows. The sulfonated diamine, 4,4′-bis(4-aminophenoxy)biphenyl-3,3′-disulfonic acid (BAPBDS), was synthesized by sulfonation of the BAPB according to our previously reported procedures[28] with some modifications.

Synthesis of 4,4′-Bis(4-nitrophenoxy)biphenyl (BNPB). The synthesis of BNPB was carried out following Scheme 1. To a 100 mL dry three-neck flask armed with Dean−Stark equipment and a condenser were added 3.724 g (20 mmol) of 4,4′dihydroxybiphenyl, 6.930 g (22 mmol) of *p*-chloronitrobenzene, 4.140 g (30 mmol) of anhydrous potassium carbonate, 20 mL of DMAc, and 10 mL of toluene. The reaction mixture was magnetically stirred and slowly heated to 140 °C, kept at this temperature for 2 h, and finally heated at 160 °C for 20 h. After cooling to room temperature, the reaction mixture was poured into 100 mL of methanol. The resulting precipitate was collected by filtration, thoroughly washed with methanol and deionized water, and dried at 60 °C in a vacuum for 20 h. 8.38 g of yellowish solid was obtained. Yield: 98%. ^{1}H NMR (DMSO-d_6, Varian Mercury Plus 400 MHz instrument): δ = 8.29 (d, J = 9.2 Hz, 4H, Ar−H), 7.82 (d, J = 8.8 Hz, 4H, Ar−H), 7.30 (d, J = 8.4 Hz, 4H, Ar−H), 7.20 (d, J = 8.8 Hz, 4H, Ar−H).

Synthesis of 4,4′-Bis(4-aminophenoxy)biphenyl (BAPB). The synthesis of BAPB was carried out by reduction of BNPB as described in Scheme 1. In short, to a 250 mL three-neck flask equipped with a dropping funnel and a condenser were added 4.28 g (10 mmol) of BNPB, 60 mL of 1,4-dioxane, 80 mL of ethanol, and 0.2 g of Pd/C. The reaction mixture was magnetically stirred and heated to 95 °C under nitrogen flow. Then, the mixture of 4 mL of hydrazine and 20 mL of ethanol was slowly added to the flask through the dropping funnel within 4 h. After the hydrazine solution was completely added, the reaction mixture was further reacted at 95 °C for an additional 20 h. After cooling to room temperature, the reaction mixture was filtered and the filtrate was poured into 1.5 L of deionized water. The resulting white precipitate was collected by filtration, thoroughly washed with deionized water, and finally dried at 60 °C in a vacuum for 20 h. 2.94 g of white solid was obtained. Yield: 80%. ^{1}H NMR (DMSO-d_6, Varian Mercury Plus 400 MHz instrument): δ = 7.53 (d, J = 8.6 Hz, 4H, Ar−H), 6.90 (d, J = 8.8 Hz, 4H, Ar−H), 6.80 (d, J = 8.8 Hz, 4H, Ar−H), 6.61 (d, J = 8.6, 4H, Ar−H), 5.02 (br, 4H, $-NH_2$).

Synthesis of 4,4′-Bis(4-aminophenoxy)biphenyl-3,3′-disulfonic Acid (BAPBDS).[28] To a 100 mL completely dried three-neck flask was added 8.0 g (22 mmol) of BAPB. The flask was cooled on an ice-bath, and then 20 mL of concentrated sulfuric acid was slowly added. During the process of acid addition, the reaction mixture was slowly stirred with a magnetic bar. After the acid addition was complete, the reaction mixture was maintained at 0 °C for 10 min. The ice-bath was removed and the reaction mixture was slowly heated to 90 °C and kept at this temperature for 5 h. After cooling to room temperature, the reaction mixture was slowly poured into 100 g of crushed ice. The solid was collected by filtration and then dissolved in 0.5 M sodium hydroxide solution. The resulting basic solution was filtered, and the filtrate was acidified with concentrated hydrochloric acid. The precipitate was collected by filtration, successively washed with deionized water and methanol, and finally dried at 120 °C under vacuum.

10.5 g of white product was obtained. Yield: 91%. ^{1}H NMR spectrum (DMSO-d_6 containing a drop of Et_3N, Varian Mercury Plus 400 MHz instrument): δ = 7.99 (d, J = 2.4 Hz, 2H, Ar−H), 7.44 (dd, J = 8.0 Hz, 2H, Ar−H), 6.77 (d, J = 8.8 Hz, 4H, Ar−H), 6.70 (d, J = 8.4 Hz, 2H, Ar−H), 6.60 (d, J = 8.8 Hz, 4H, Ar−H), 4.91 (br, 4H, $-NH_2$).

Polymer Synthesis and Membrane Preparation. The polycondensation reaction was performed using the steps indicated in Scheme 2. To a 100 mL completely dried three-neck flask were added 0.792 g (1.5 mmol) of BAPBDS, 10.0 mL of *m*-cresol, and 0.60 mL of Et_3N under nitrogen flow with magnetic stirring. After BAPBDS was completely dissolved, 0.184 g (0.5 mmol) of BAPB, 0.536 g (2.0 mmol) of NTDA, 0.488 g (4.0 mmol) of benzoic acid, and 0.516 g (4.0 mmol) of isoquinoline were added to the flask. The mixture was stirred at room temperature for a few minutes and then heated at 80 °C for 4 h and 180 °C for 20 h. After cooling to room temperature, the highly viscous solution mixture was diluted with an additional 5.0 mL of *m*-cresol and then poured into 150 mL of acetone with stirring. The fiber-like precipitate was collected by filtration, washed with acetone, and dried at 80 °C in a vacuum for 10 h. The IR spectrum of the polymer, presented in Figure 1 of the Supporting Information, clearly shows the characteristic absorption bands of the stretch of imide carbonyl groups (1712 and 1666 cm^{-1}), the stretch of C−N (1349 cm^{-1}), and the stretch of sulfonic acid groups (1233, 1087, 1014 cm^{-1}), suggesting the formation of the sulfonated polyimide structure.

The membranes prepared from *m*-cresol solutions by casting, at 110 °C, were soaked in methanol at 50 °C for 5 h first, and then in high vacuum, at 80 °C for 10 h. The membranes were immersed in 1 M hydrochloric acid at room temperature for three days. After their removal from the solution, the membranes were washed several times with deionized water to eliminate traces of free acid in them and dried at 120 °C for 10 h under vacuum. Then, a weighed sample of dried membrane was immersed in 1 N solution of NaCl and the ion-exchange capacity (IEC) was obtained by titration with a 0.01 M hydroxide solution. The value of the IEC was 2.08 Eq/kg, and the water uptake of the membrane equilibrated with water was 0.99 kg/kg dry membrane. The thickness of the membranes lied in the vicinity of 50 μm.

Conditioning of Membranes with Different Water Contents. Membranes in the acid form were immersed in a 1 N lithium chloride solution to exchange protons for lithium according to the scheme

$$R{-}SO_3H + Li^+ \rightarrow R{-}SO_3Li + H^+ \quad (1)$$

The membranes, washed several times with deionized water to eliminate excess lithium chloride and the hydrochloric acid formed in the exchange reaction, were dried. The preparation of membranes with different water contents was first intended by conditioning the dried membrane in an atmosphere with the relative humidity of interest. However, the kinetics of the water sorption process was found to be very slow, in such a way that the time necessary to get equilibrium conditions was prohibitively long. To circumvent this problem and taking into account that the desorption process is rather rapid, the water saturated membrane was kept in the conditioning atmosphere of interest for about 24 h in order to ensure that the distribution of the water in the membrane was at equilibrium.

Nuclear Magnetic Resonance Measurements. The NMR measurements were performed in a Bruker Avance 400 spectrometer equipped with a 89 mm wide bore, 9.4 T superconducting magnet (Larmor frequencies of ^{1}H, ^{7}Li, and ^{6}Li at 400.14, 155.51, and 58.88 MHz, respectively). The ^{1}H and ^{7}Li diffusion reported data were acquired at 25 ± 0.2 °C with a Bruker diffusion probe head, Diff60, using 90° radiofrequency (rf) pulse lengths between 6.4 and 11.0 μs. A pulsed field gradient stimulated spin echo pulse sequence was used.[29] The time between the first two 90° rf pulses (the echo time), τ_1, was 3.12 ms. The apparent diffusion coefficients of ^{1}H and ^{7}Li, D, were measured varying the amplitude of the gradient pulse between 0 and 22 T m^{-1}. The diffusion time, t_D, and length of the gradient pulses, t_g, were 60 and 2 ms, respectively, unless specified otherwise. Measurements at different diffusion times were also performed to assess its effect on D. The repetition rate was always 5 times the spin−lattice relaxation time, T_1, of the nuclei being observed. The total acquisition time for these experiments varied from 10 min to 24 h. The decay of the echo amplitude was monitored typically to, at least, 50% of its initial value, and the apparent diffusion coefficient was calculated by fitting a monoexponential function to the decay curve. Previously, the magnetic field gradient was calibrated as described elsewhere.[30]

^{1}H, ^{7}Li, and ^{6}Li NMR spectra of membranes with various degrees of hydration were acquired with a standard Bruker double resonance 4 mm cross-polarization/magic angle spinning NMR probehead using 90° for ^{1}H and ∼35° for ^{7}Li and ^{6}Li, rf pulse lengths between 2.0 and 3.0 μs, and recycle delays of 10 s. Samples were placed in 4 mm zirconia rotors and spun at the magic angle at a rate of 5−10 kHz. In addition, spectra with static samples were acquired. The ^{1}H and ^{7}Li/^{6}Li spectra were externally referenced to TMS and 1.56 M lithium chloride aqueous solution, respectively.

The ^{1}H and ^{7}Li longitudinal relaxation times, T_1, of lithium ions and water protons in membranes were estimated using an inversion−recovery ($\pi - t_i - \pi/2$) pulse sequence.

X-ray Characterization. Small-angle X-ray scattering (SAXS) experiments were carried out on a Bruker AXS Nanostar small-angle X-ray scattering instrument, using Cu Kα radiation (1.542 Å) produced in a sealed tube. The scattered X-rays were detected on a two-dimensional multiwire area detector and could be converted to one-dimensional scattering by radial averaging and represented as a function of momentum transfer vector q ($q = 4\pi \sin\theta/\lambda$) in which θ is half the scattering angle and λ is the wavelength of the incident X-ray beam. The raw intensity data [$I(q)$] were corrected for detector linearity, sample absorption, background scattering, and changes in incident beam intensity. WAXS patterns were recorded in the reflection mode, at room temperature, by using a Bruker D8 Advance diffractometer provided with a Goebel mirror and a PSD Vantec detector (from Bruker, Madison, WI). Cu Kα radiation (1.542 Å) was used, operating at 40 kV and 40 mA. The equipment was calibrated with different standards. The diffraction scans were collected within the range of 2θ from 2 to 40° with a 2θ step of 0.024° and 0.1 s per step.

Conductivity Experiments. The measurement of the conductivity of membranes with different water contents was performed with a Novocontrol broadband dielectric spectrometer (Hundsagen, Germany) integrated by a SR 830 lock-in amplifier with an Alpha dielectric interface in the frequency range 10^{-2}−10^7 Hz. The electrodes used were gold disks of 10 mm diameter. The temperature was controlled by a nitrogen jet (QUATRO from Novocontrol) with a temperature error of 0.1 K during every single sweep in frequency. The equivalent

electric circuit of a cation-exchange membrane is a resistance, R_0, representing the ohmic resistance of the membrane in series with a circuit that accounts for the polarization of the membrane made up of a resistance R_p in parallel with the capacitor of capacity C. The impedance of the circuit is given by

$$Z^* = R_0 + \frac{R_p}{1 + j\omega R_p C} \tag{2}$$

The value of R_0 was obtained by the Nyquist method or Z'' vs Z' plots in the limit $\omega \to \infty$. An alternative procedure is the Bode method for which R_0 is the value of the modulus of the complex impedance, $|Z^*|$, at which $\phi = \tan^{-1}(Z''/Z')$ reaches a maximum. Strictly speaking, the capacitor in the equivalent circuit should be replaced by a constant phase element.[31] However, this element does not change the results for the limit condition ($\omega \to \infty$) from which the ohmic resistance is estimated.

EXPERIMENTAL RESULTS

A. Conductivity. Illustrative Nyquist and Bode plots for the membrane in the lithium form saturated with water are shown in Figure 2 of the Supporting Information. The two plots yield independently the ohmic resistance of the membranes to lithium cation transport. The conductivity of the membranes was obtained from the ohmic resistance of the membranes R_0 by means of the following expression

$$\sigma = \frac{l}{R_0 A} \tag{3}$$

where A is the area of the membrane in contact with the electrodes and l its thickness. As a result of evaporation occurring in the conditioned membranes during the conductivity measurements for membranes with nominal water content lying in the range $10.7 < \lambda < 26.5$, where λ is the number of molecules of water per fixed ionic group, the values of the conductivity are somewhat uncertain. However, the measurements in the fully hydrated membrane ($\lambda = 26.5$) were carried out in an electrode cell containing deionized water in such a way that the conductivity estimation was highly reproducible. The same occurs with the dry membrane ($\lambda = 0$) and with the membrane with $\lambda = 8$. The dependence of the conductivity of membrane in the lithium form on the water content, presented in Figure 1, shows a relatively slight diminution with high water content. However, for $\lambda < 10$, the decrease in humidity causes a sharp decrease of the Li^+ conductivity.

Under an electric field $-dV/dx$, 1 mol of the mobile ionic species i in the membrane phase undergoes a force $-z_i F\, dV/dx$, where z_i is the valence of the ionic species i and F is Faraday's constant. The mobile species are accelerated until a velocity u_i is reached at which the acceleration force is compensated by the friction force $u_i\chi_i$, where χ_i is the friction coefficient per mole of the species i against the membrane surroundings, in such a way that steady state conditions are reached. In this condition, the flux of species i is $J_i = c_i u_i = -F(c_i z_i/\chi_i)\, dV/dx$. Taking into account that the current density is $j = F\Sigma_i z_i J_i$ and the Einstein's relationship $\chi_i = RT/D_{\sigma i}$, where $D_{\sigma i}$ is the diffusion coefficient of the charge i, the conductivity of the membranes can be written as

$$\sigma = -\frac{j}{dV/dx} = \frac{F^2 \sum_i c_i z_i^2 D_{\sigma i}}{RT} \tag{4}$$

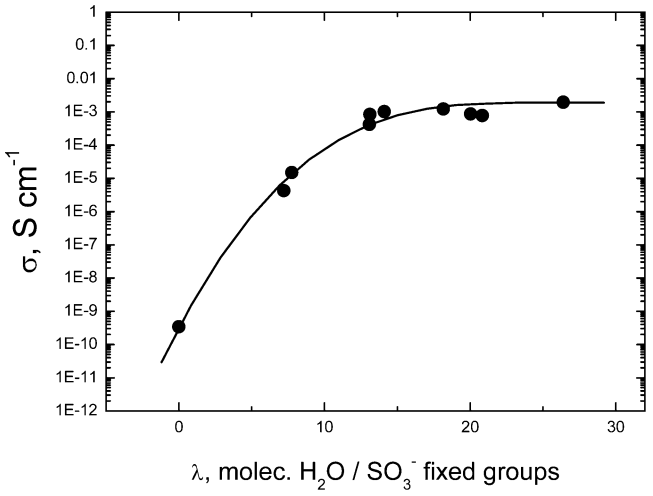

Figure 1. Dependence of the conductivity on the humidity of the membranes.

In the conductivity measurement conditions used in this work, mobile co-ions are excluded from the membrane, and taking into account that the counterions are monovalent, the diffusion coefficient of lithium cation D_σ can be written as[32]

$$D_\sigma = \frac{RT\sigma}{cF^2} \tag{5}$$

In this expression, c is the concentration of Li^+ in the wet membrane calculated as $c = \rho X/(1 + \rho w)$, where ρ and X are respectively the density of the dry membrane and the moles of fixed ions per gram of dry membrane, while w is the water content per gram of dry membrane. The diffusion coefficient of Li^+ was calculated by means of eq 5, and the pertinent results for membranes with different water content are shown in Figure 2. As expected, the dependence of the diffusion coefficients on water follows the same trends as the conductivity.

B. ^{7}Li, ^{6}Li, and ^{1}H Solid State NMR Results. Prior to performing the diffusion measurements, the ^{7}Li and ^{1}H solid state NMR spectra of membranes with varying degree of

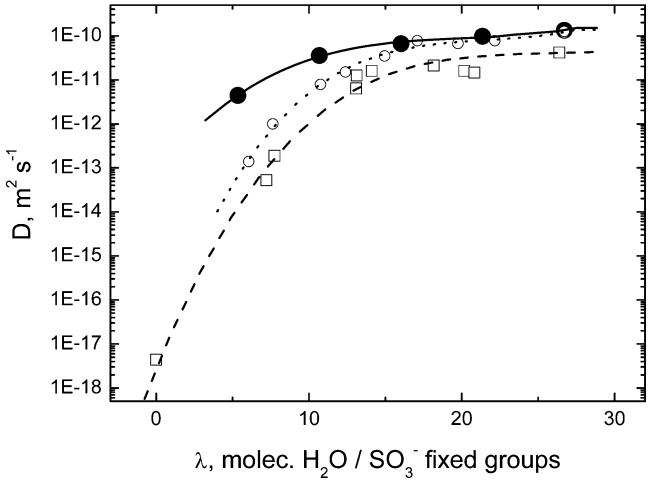

Figure 2. Variation of the diffusion coefficient of Li^+ with the water content of the SNCPI membranes. The diffusion coefficients were obtained by ^{7}Li PFG-NMR (open circles), conductivity (open squares), and MD simulation techniques (filled circles).

hydration were acquired. The ^{7}Li static NMR spectra exhibited a single peak with a full width at half-height, $\nu_{1/2}$, increasing with decreasing water content, as shown in Figure 3 of the Supporting Information. The ^{1}H static NMR spectra showed similar behavior, as illustrated in Figure 4 of the Supporting Information. The results are summarized in Table 1. As

Table 1. Full Width at Half-Height of ^{7}Li and ^{1}H Static Solid State NMR Spectra Corresponding to Membranes with Varying Water Content *w* Expressed in Terms of g of H_2O/g of dry membrane

w	^{7}Li $\nu_{1/2}$ (Hz)	^{1}H $\nu_{1/2}$ (Hz)
1.00	220	630
0.50	540	1060
0.13	670	2400
0	3300	

expected, the spinning of the samples at the magic angle lead to a reduction of the line-width of the observed peak in the ^{7}Li spectra. The ^{6}Li spectra (see Figure 5 of the Supporting Information) are similar to those of ^{7}Li. A single peak is observed with increasing broadening as the water content in the membranes decreases. Also, a slight displacement of the chemical shift from 0 to −0.55 ppm is noticed. The proton spectra of membranes with low water content (λ = 4.5 molecules of water per fixed ionic group), shown in Figure 3, spun at 10 kHz, showed a peak associated with the polymer at 7 ppm, in addition to the water peak at 4.5 ppm. The ^{1}H spectrum of the apparently dry membrane exhibits the peak of polymer protons and a narrow peak at about 0 ppm not identified. This peak could be attributed to a residual amount of

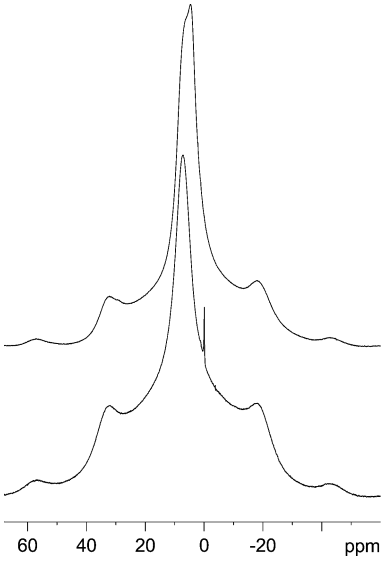

Figure 3. ^{1}H MAS NMR spectra corresponding to membranes with λ = 4.5 molec. H_2O/SO_3^- fixed groups (top) and 0 (bottom). The water content was obtained from the weights of the wet membrane and the membrane dried by vacuum at room temperature. The top spectrum shows a peak at 4.5 ppm associated with removable sorbed water and a shoulder attributed to the polymer. The bottom spectrum shows the peak corresponding to the polymer at 7 ppm and the peak at 0 ppm attributed to protons of nonremovable water. Spinning side bands associated with protons of the polymer membrane are observed as ± multiples of the spinning rate of 10 kHz.

the solvent used in the preparation of membranes and protons of nonremovable water, in highly shielded environment.[33] Notice that the thermogravimetric curve of the apparently dried membrane, shown in Figure 6 of the Supporting Information, exhibits a 5% weight loss after reaching the membrane 100 °C of temperature. It is worth noting that the thermograms show that the $-SO_3Li$ ionic group is stable above a temperature of about 200 °C, at which sulfonic acid groups undergo strong degradation in acidic membranes.

C. ^{7}Li and ^{1}H PFG-NMR Results. As indicated above, the effective transverse or spin−spin relaxation time, $T_2^* = 1/\pi\nu_{1/2}$, of ^{7}Li and ^{1}H in these membranes is short. Since the PFG methods are based on the observation of an echo, the rapid decay of the signal (short T_2^*) leads to a significant reduction in the signal-to-noise ratio of the spectrum, thus limiting the practical range of some experimental parameters, i.e., diffusion times, and requiring an increase in signal averaging to improve detection. Thus, a stimulated spin echo sequence was chosen because it allows short echo times and the diffusion time t_D is limited by T_1. The results of T_1 measurements are summarized in Table 2. The values of ^{7}Li T_1 measured varied from 2.89 to

Table 2. ^{7}Li and ^{1}H Spin−Lattice NMR Relaxation Times T_1 Corresponding to Membranes with Varying Water Content *w* Expressed in Terms of g of Water/g of Dry Membrane, at 25 °C[a]

w	^{7}Li T_1 (s)	*w*	^{1}H T_1 (s)
1.00 (26.7)	2.89	0.961 (25.7)	0.65
0.83 (22.2)	2.31	0.784 (20.9)	0.5
0.74 (19.8)	1.73	0.51 (13.6)	0.3
0.74[b] (19.8)	1.73	0.31 (8.3)	0.2
0.64 (17.1)	1.74	0.196 (5.2)	0.2
0.56 (15.0)	1.44	0.107 (2.9)	0.2
0.464 (12.4)	1.15		
0.403 (10.8)	0.72		
0.286 (7.6)	0.40		
0.227 (6.0)	0.36		

[a]Between brackets, values of λ (molecules of water per sulfonate group). In these and other NMR experiments, the weight of the dry membrane was taken as that of the wet membrane dried in high vacuum at room temperature for 24 h. [b]Same sample, 9 days after first measurement.

0.36 s, and the corresponding values for ^{1}H were in the range 0.65−0.2 s. Taking these results into consideration, a value of t_D = 60 ms was chosen for the *D* measurements described, although the influence of t_D on the value of *D* for ^{7}Li was assessed.

The PFG-NMR methods allow the determination of diffusion coefficients by measuring the signal attenuation with increasing values of magnetic field gradients, *g*, and t_D, as first shown by Stejskal and Tanner[29]

$$A(g) = A(0)\exp(-mD) \quad (6)$$

where $A(g)$ and $A(0)$ are the amplitude of the echo in the presence of a gradient pulse with amplitude *g* and 0, respectively, $m = (\gamma g t_g)^2(t_D - t_g/3)$, where γ is the gyromagnetic ratio of the nucleus being observed, t_g represents the duration of the magnetic field gradient pulse, and *D* is the diffusion coefficient. Figure 4 illustrates the results of the fit to eq 6 for ^{7}Li and ^{1}H attenuation plots corresponding to the membranes described in the legend. The results of the PFG-

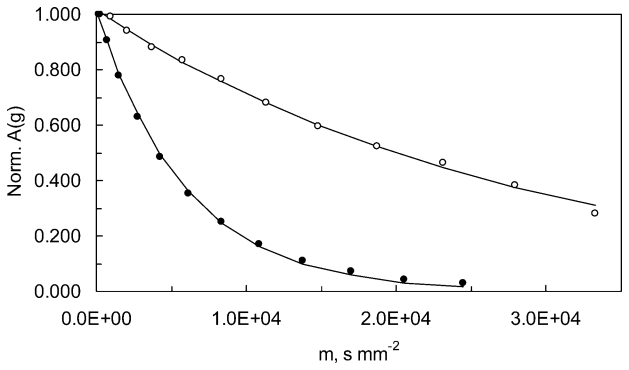

Figure 4. Plot of normalized $A(g)$ vs m (s mm^{-2}) corresponding to ^{7}Li (open circles) and water ^{1}H (closed circles) in membranes measured at 25 °C with a diffusion time, t_D, equal to 60 ms. The water content expressed in terms of λ (molec. H_2O/SO_3^- fixed groups) was 15.0 (^{7}Li) and 13.6 (^{1}H). The duration of the gradient pulse, t_g, was kept constant at 2 ms, and the amplitude of the field gradient, g, in T m^{-1}, was varied between 0.10 and 3.60. The solid line corresponds to a monoexponential (eq 6) fit.

NMR measurements for ^{7}Li and ^{1}H (H_2O) are summarized in Figures 2 and 5, respectively.

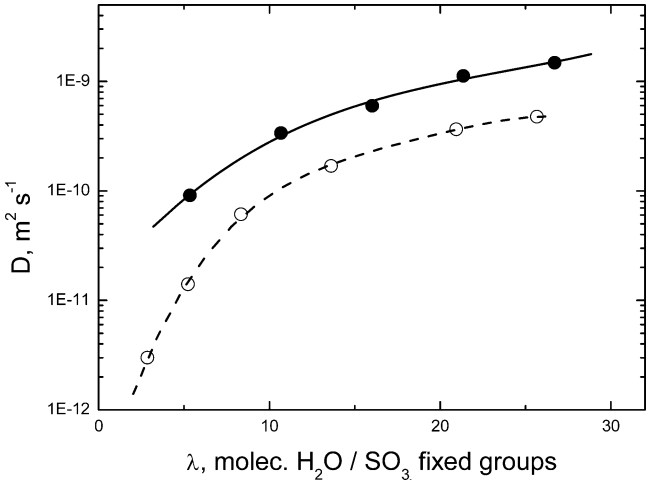

Figure 5. Variation of the diffusion coefficient of water obtained by MD simulation (filled circles) and PFG-NMR (open circles) with the water content of the membranes.

The influence of the diffusion time on the value of the ^{7}Li diffusion coefficient was studied varying t_D between 30 and 1000 ms in membranes exhibiting sufficiently long values of T_1, and the results are shown in Table 3. No significant effect of t_D on the values of D_{Li} was observed.

In parallel with the measurements of the diffusion coefficients of ^{1}H (H_2O) and ^{7}Li in the membranes carried out by PFG-NMR techniques, these parameters were also measured in free LiCl solutions and the pertinent results are plotted as a function of the salt concentration in Figure 6. In general, the increase of concentration in the solutions tends to decrease the mobility of ^{7}Li and ^{1}H.

D. X-ray Diffractograms. The SAXS and WAXS diffractograms of the wet membranes in the lithium form are shown in Figure 7. The SAXS of the fully hydrated membranes do not exhibit the ionomer peak in the range of q measured (q < 2 nm^{-1}). The low angles of the WAXS diffractograms of the fully

Table 3. ^{7}Li PFG NMR Diffusion Measurements in Membranes with Varying Water Content at 25 °C and Variable Diffusion Time t_D[a]

w	t_D (ms)	^{7}Li $D \times 10^{11}$ (m^2 s^{-1})
1.00	60	11.7
	600	10.6
	1000	10.0
0.74	30	6.76
	60	6.72
	150	6.83
	300	6.63
	600	6.62
0.56	30	3.48
	60	3.49
	600	3.47
0.28_6	60	0.10
	120	0.10

[a]The water content w is expressed in terms of g of water/g of dried membrane. The duration of the gradient pulse was kept constant at 2 ms.

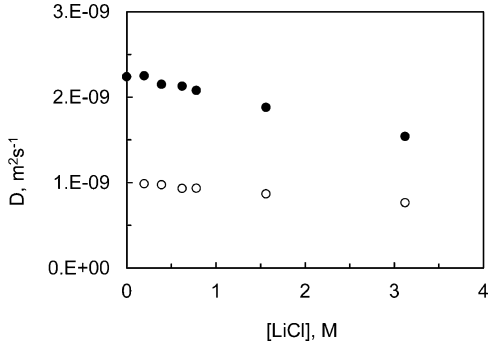

Figure 6. Variation of the diffusion coefficient of water ^{1}H (closed circles) and ^{7}Li (open circles), measured by PFG-NMR, in free LiCl aqueous solutions.

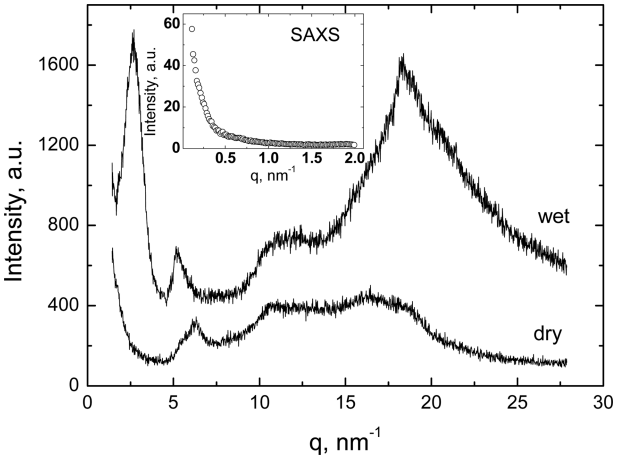

Figure 7. Illustrative WAXS diffractograms for the wet and dry membranes in the lithium form. In the inset, the SAXS diffractogram of the wet membrane for $q \leq 2$ nm^{-1} is shown.

hydrated membrane present the ionomer peak centered at q = 2.6 nm^{-1}. As the water content of the membranes decreases, the intensity of the peak decreases and its location is shifted to higher values of q. That peak is absent in the diffractograms of membranes with λ < 3.5 as well as in completely dry

membranes. Wet and dry membranes present peaks at higher values of q, which become better resolved in the wet membranes. The diffractograms of the membranes in the acid and lithium forms are similar.

E. Computational Details and Results. Bulk structures of five chains of NTDA-BAPBDS/BAPB (3/1) of molecular weight 2878.65 g/mol with 30 lithium ions and water absorbed (Table 4) were generated and simulated by means of the

Table 4. Dimensions and Composition of the Computing Cell

cell	g of H_2O/g of dry membrane	λ, molec. H_2O/SO_3^- fixed group	n H_2O	L cell (Å)	ρ (g/cm^3)
SNCPI-00	0	0	0	26.1136	1.36
SNCPI-20	0.2	5.3	165	28.1665	1.31
SNCPI-40	0.4	10.6	325	30.1309	1.24
SNCPI-60	0.6	15.9	485	32.2283	1.16
SNCPI-80	0.8	21.2	650	34.3122	1.08
SNCPI-100	1.00	26.7	850	36.2186	1.02

Accelrys commercial software[34] using the COMPASS force field. The atomic charges were force field assigned. van der Waals and Coulombic nonbonding interactions were calculated, respectively, by atom based (cutoff distance of 12.5 Å) and Ewald (accuracy of 0.001 kcal/mol) as summation methods. The cell constructions were followed by NPT molecular dynamics of 300 ps. Berendsen thermostat and barostat methods, with a decay constant of 0.1 ps, were used to maintain a constant temperature and pressure of 298 K and 0.1 MPa, respectively. The last obtained conformation, with final density (Table 4), was used for NVT simulation at 298 K where, after the first 100 ps, 1 ns were collected for further analysis. A time step of 1 fs (i.e., 10^{-15} s) was used for the integration of the atomic motion equations. In what follows, the simulation cells will be called SNCPI-XX, where XX represents g of water per 100 g of dry membrane.

A van der Waals volume mapping of the SNCPI cells is shown in Figure 8. The red color represents the atoms of the polyelectrolyte, whereas the blue color corresponds to molecules of water. For the SNCPI-20 (λ = 5.3) cells, the water is located in very small domains and across the polyelectrolytes as the decreasing of the intensity of the red color in certain places of the cell occupied by the polyelectrolyte show. However, as the amount of water increases, the size of the water domains also increases, favoring the formation of percolation paths through which Li and water diffusion may occur.

Diffusion coefficients of either Li^+ or water were carried out from the computed trajectory of the particles of interest using the Einstein−Stokes expression

$$D = \frac{1}{6} \lim_{t\to\infty} \frac{\langle [\mathbf{r}(t) - \mathbf{r}(0)]^2 \rangle}{t} \tag{7}$$

where $\mathbf{r}(t)$ indicates the position of a given particle at time t. Values of mean-square displacements (MSD) of the trajectories, $\langle [\mathbf{r}(t) - \mathbf{r}(0)]^2 \rangle$, for cells with different water contents are shown in Figures 7 and 8 of the Supporting Information for lithium cations and water, respectively. At short times, the derivatives of the MSDs with respect to time depend on time, reflecting nonsteady state conditions. After a certain time, which decreases as the water content of the cell increases, the slope of the curve log MSD vs t is the unit, a fact that reflects steady state conditions. In the case of the particles of Li^+, much more time is necessary to reach steady state conditions. Thus, in the case of the cells SNCPI-00 (λ = 0), SNCPI-20 (λ = 5.3), and SNCPI-40 (λ = 10.6), those conditions are apparently not reached. Simulated values of $D(Li^+)$ and $D(H_2O)$ obtained, respectively, from Figures 7 and 8 of the Supporting Information are plotted as a function of the

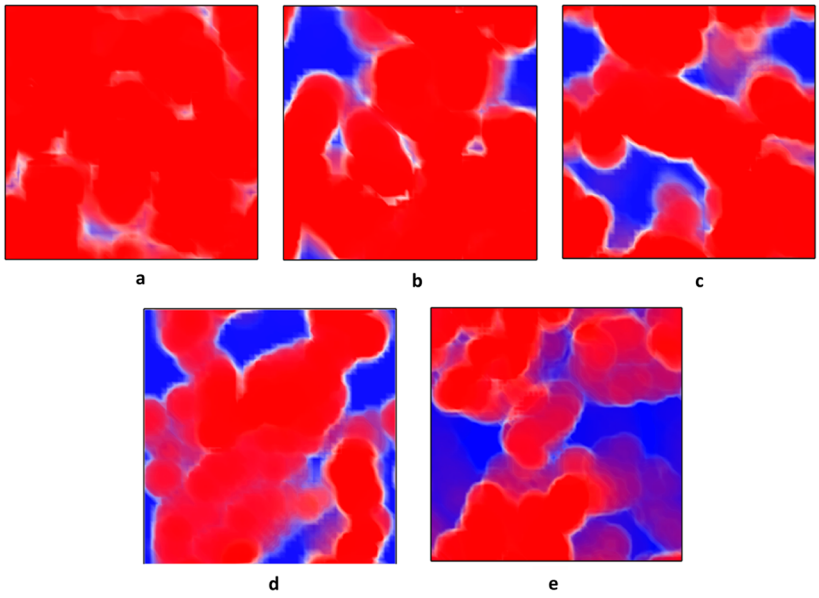

Figure 8. Mapping with van der Waals volume showing the polyelectrolyte (red) and water (blue) for the cells: SNCPI-20 (λ = 5.3) (a), SNCPI-40 (λ = 10.6) (b), SNCPI-60 (λ = 15.9) (c), SNCPI-80 (λ = 21.2) (d), and SNCPI-100 (λ = 26.7) (e). The units of λ are molec. water/SO_3^- fixed groups.

water content in Figures 2 and 5, respectively. An inspection of the curves shows that the simulated values of $D(Li^+)$ fit rather well to the values obtained for this quantity using ^{7}Li PFG-NMR techniques for $\lambda > 15$. For $\lambda < 15$, the simulated values of $D(Li^+)$ fall above those obtained by RMN and the departure between them increases as the water content of the membranes decreases. The cause of this discrepancy might be the prohibitively long computing time necessary to reach steady state conditions in membranes with low water content.

DISCUSSION

Although the physicochemical characteristics of cations in cation-exchange membranes depend on the collective interactions between the cation and water molecules in the pores of the membranes, the structure of water and its effect on the equilibrium and dynamic properties of these systems are not clearly understood. This is so even in the case of free dilute solutions.[35] The distribution of water in the pores of the naphthalenic copolyimide cation-exchange membrane was carried by computing intermolecular pair correlation functions $g_{AB}(r)$ that represent the probability of finding a pair of particles AB at a distance $r \pm \Delta r$ normalized with respect to the probability expected for a completely random distribution at the same density. The values of g_{AB} were computed by means of the following expression[36]

$$g_{AB}(r) = \frac{V\langle \sum_{i\neq j} \delta(\mathbf{r} - |\mathbf{r}_{Ai} - \mathbf{r}_{Bj}|)\rangle}{(N_A N_B - N_{AB})4\pi r^2 \Delta r} \quad (8)$$

where V is the volume of the shell, $\mathbf{r}_{Ai}$ and $\mathbf{r}_{Bj}$ represent the positions of the particles i of kind A and j of kind B in such a way that $|\mathbf{r}_{Ai} - \mathbf{r}_{Bj}|$ is the distance between them. The term $\delta(\mathbf{r} - |\mathbf{r}_{Ai} - \mathbf{r}_{Bj}|)$ is set to unit when $\mathbf{r} - |\mathbf{r}_{Ai} - \mathbf{r}_{Bj}| \leq \Delta r$ and zero otherwise. Illustrative plots showing $g_{Li^+\cdots O(H_2O)}(r)$ and $g_{O(SO_3)\cdots O(H_2O)}$ for cells with different water content are presented in Figures 9 and 10 of the Supporting Information. The average radii for the primary and secondary hydration shells $Li^+-O(H_2O)$ were estimated, respectively, as the radii at which the function $g_{r\cdots O}(r)$ reaches the first and second minima. The value estimated for the radius of the first shell for the SNCPI-100 (λ = 26.7) cell was 2.85 Å, in rather good agreement with the value of 2.775 Å computed for Li^+ in very dilute LiCl solutions,[35] whereas that of the second shell amounts to 5.63 Å. The radii for the first and second shells of the fixed anionic group $O(SO_3)\cdots O(H_2O)$ were, respectively, 3.97 and 6.43 Å. It is worth noting that the radius of the first shell is very close to that computed for $Cl^-\cdots O(H_2O)$, in very diluted LiCl solutions (3.98 Å).[35]

Coordination or hydration numbers of cations and fixed anions can be obtained from $g(r)$ by means of the following equation

$$n_{x\cdots z} = 4\pi \frac{N_z}{V} \int_0^{r_1} g_{x\cdots z}(s) s^2 \, ds \quad (9)$$

where $n_{x\cdots z}$ is the number of particles x coordinated to particle z within a radius r_1 of the first shell, whereas V and N_z represent, respectively, the volume and the total number of particles in the cell. Integration between r_1 and the radius of the second shell r_2 in the distribution function, if it exists, yields the hydration number in the second shell. Values of the coordination numbers for $Li^+\cdots O(H_2O)$ in the first and second shells are shown in Table 5. It can be seen that the hydration number in the first shell increases with the water content in the membrane from 1.88 for the SNCPI-20 (λ = 5.3) membrane to 2.62 for the SNCPI-100 (λ = 26.7) membrane. One would expect that some water that forms part of dynamic tetrahedral water networks in the hydrophilic domains will be tetrahedrally oriented around Li^+ ions.[35,37] For very dilute LiCl solutions, that is the case, but as the concentration increases, the hydration number drops to a number close to 3 because the Cl^- anion together with three molecules of water coordinate the Li^+ cation.[35] In any case, the distribution of cations in the wet membranes may be more complex than the NMR and simulation results suggest. In earlier work, we have observed the presence of isolated and clustered Na ions in sulfonated polynorborne membranes functionalized with sulfonated dicarboxiimide side groups using ^{23}Na solid state NMR.[38] Thus, it seems likely that similar populations of Li cations could be present in the polyimide membranes subject of the present work. However, only a single peak is observed in the ^{7}Li and ^{6}Li solid state NMR spectra corresponding to these membranes. The relatively narrow chemical shift dispersion of the ^{7}Li and ^{6}Li NMR spectra compared to that of ^{23}Na hampers a direct observation (discrimination) of these ionic species.

Table 5. Hydration Number for Lithium Cations and Sulfonate Fixed Anions in the Cells as a Function of the Water Content[a]

cell	1st (Å)	n_1	2° (Å)	n_2	$R = n_2/n_1$
		$Li^+\cdots(O)H_2O$			
SNCPI-20	2.85	1.88	5.63	5.79	3.08
SNCPI-40	2.85	2.35	5.63	8.32	3.54
SNCPI-60	2.85	2.45	5.63	9.85	4.01
SNCPI-80	2.85	2.40	5.63	9.84	4.10
SNCPI-100	2.85	2.62	5.63	10.69	4.08
		$(O)SO_3\cdots(O)H_2O$			
SNCPI-20	3.97	2.16	6.43	8.70	4.03
SNCPI-40	3.97	2.78	6.43	12.18	4.39
SNCPI-60	3.97	3.14	6.43	14.21	4.54
SNCPI-80	3.97	3.19	6.43	14.64	4.59
SNCPI-100	3.97	3.32	6.43	15.07	4.54

[a]The values of the second and fourth columns of the table correspond to the respective radii of the first and second shells.

As the results collected in Table 5 show, the anion hydration number $O(SO_3)\cdots O(H_2O)$ also increases with the water content of the membrane. The values of this quantity are 2.16 and 3.32 for the SNCPI-20 (λ = 5.3) and SNCPI-100 (λ = 26.7) membranes, respectively. It is worth noting that the value of the anion hydration number is nearly 50% of that computed for Cl^- in LiCl solutions, where the value of this quantity lies in the vicinity of 7.5 and it is nearly independent of the concentration of the solution.[35] The value of this quantity measured by neutron scattering experiment is 5.5.[39] The ratio of the number of molecules of water associated with the particle i between the second and first shell is given in Table 5. It can be seen that the ratio for Li^+ increases with the water content of the membranes. Thus, the values associated with the SNCPI-20 (λ = 5.3) and SNCPI-100 (λ = 26.7) membranes are 3.08 and 4.08, respectively. The same occurs for the $-SO_3^-$ anion, but in this case, the extreme values are 4.03 and 4.54, respectively. It is worth noting that these ratios are higher than those computed for 0.2 M LiCl solutions which amount to 4.17 and 3.52 for the cations and anions, respectively. This is a consequence of the

fact that the hydration number for the cation and the anion in the membrane is lower than in the case of free dilute solutions.

Interactions of water and ionic groups in the membranes are reflected in the variation of the diffusion coefficient of water with the water content of the membranes, presented in Figure 5. The dependence of the logarithm of $D(H_2O)$ on the water content of the membrane reflects that of the diffusion coefficient of Li^+, measured by the same technique. It seems that the diffusion of water taking place through the network structure is disrupted by the interactions of these molecules with both the mobile and fixed ionic groups of the membranes. The rather sharp fall of $D(H_2O)$ for $\lambda < 12$ is likely the consequence of an increase of such interactions that also lead to a decrease in the swelling of the membrane. The water–ion interactions are put in evidence in Figure 6 where the diffusion coefficient of water in free LiCl solutions is plotted as a function of the salt concentration. It can be seen that the diffusion coefficients of ^7Li and ^1H (H_2O) undergo, respectively, a slight and moderate decrease with increasing salt concentration in the free solution. As can be seen in Figure 5, the values of the diffusion coefficient of water computed by MD techniques for membranes with different water contents are somewhat higher than those measured by the ^1H PFG-NMR technique. However, it is remarkable that the ratio between the values of these parameters obtained by these techniques is roughly independent of the water content of the membranes.

The structure of hydrated cation-exchange monomers in the acid form is still an unresolved issue, even in the case of the widely studied Nafion membranes. The evidence of ionic aggregation in the hydrated ionic membranes is illustrated by the so-called ionomer peak observed by small-angle scattering (SAXS) at a scattering angle corresponding to a Bragg spacing of 2–6 nm. The ionomer peak in hydrated Nafion has been variously attributed to spherical inverted-micelle-water-clusters, layered structures, channel networks, and polymer bundles.[40] The hydrophobic perfluorinated skeleton of Nafion combined with the strong acidity ($pK = -6$) of the perfluorsulfonic acid facilitates, in the presence of water, some hydrophobic–hydrophilic nanoseparation. Simulation computations of published SAXS data carried out recently by Schmidt-Rohr and Cheng[40] suggest that the ionomer peak of Nafion arises from long parallel but otherwise randomly packed water chains surrounded by partially hydrophilic side branches, forming inverted micelle cylinders. If the microstructure of flexible polyelectrolytes such as Nafion is not well understood, the understanding of the microstructure of membranes integrated by rigid polyelectrolytes such as polyimides, polysulfones, polyetherether ketones, etc., is even worse. The high rigidity of the chains accompanied by the lower acidity of the sulfonic acid groups hinders the segregation of hydrophilic moieties from hydrophobic ones to form hydrophilic paths through which cation transport takes place. SAXS diffractogram patterns of polyetherether ketones exhibit the ionomer peak centered at q = 1.5 nm^{-1} corresponding to a spacing of approximately 4 nm.[27] The ionomer peak is shifted to lower values of q for block naphthalenic copolyimide membranes containing 4,4′-oxidianiline residues in their structures.[41] In this case, the characteristic segregation distances are about 30 nm, ca. 10 times those reported for usual ionomers, a result that was attributed to the block character of the polymers. Moreover, the periodicity distances are the same for H^+ and all the alkaline counterions (Li^+, Na^+, Rb^+, Cs^+) and therefore independent of their size.[41]

As indicated before, the SAXS difractograms of the wet random copolyimides studied in this work do not present the ionomer peak at $q < 2$ nm^{-1}. However, the WAXS diffractograms of the fully hydrated membrane, shown in Figure 9, exhibit the ionomer peak at q = 2.66 nm^{-1} that

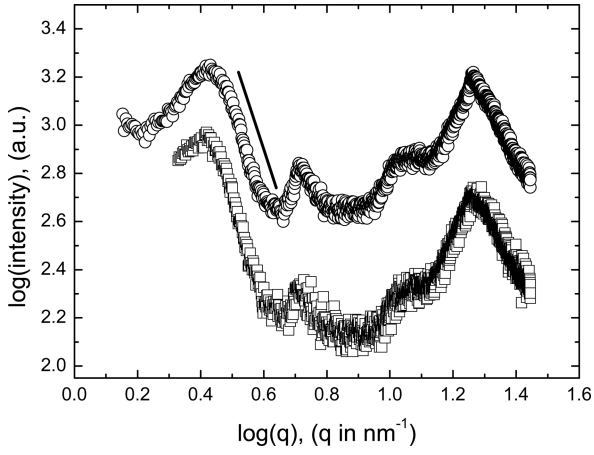

Figure 9. X-ray diffractograms of the fully hydrated membranes in the lithium (open circles) and acid (open squares) forms. The straight line represents the Porod regime $I(q) \sim q^{-4}$.

corresponds to a segregation distance of about 2.35 nm. This size is only slightly lower than the end-to-end distance of the extended sulfonated repeat unit of the copolyimide, shown in Figure 11 of the Supporting Information, which amounts to 2.46 nm. Moreover, the segregation distance of the hydrated copolyimide is only 8% of that reported for sulfonated block copolyimides.[41] It is worth noting that the block copolyimide membrane with IEC 2.15 Eq/kg dry membrane to which we have referred before presents a conductivity of 0.027 S/cm, nearly 10 times that of the membrane studied in this work with nearly the same IEC. This fact highlights the great importance of the hydrophilic segregation on the conductivity of ion-exchange membranes.

The ionomer peak for the membranes in the acid form is centered at nearly the same value of q as their counterparts in the lithium form (see Figure 9). The curves of Figure 10 show that the decrease of the water content in the membrane shifts the peak to higher q. On the other hand, although the intensity of the peak is given in arbitrary units, the fact that the X-ray diffractograms were performed in the same sample suggests that, as expected, the intensity of the ionomer peak decreases with the water content of the membrane. The scattering intensity at high scattering angles (Porod regime) of the fully hydrated membranes nearly obeys the scaling law $I(q) \sim q^{-4}$. This means that the separation between hydrophobic and hydrophilic domains is not a fractal in the more hydrated membranes but approaches a smooth surface.[42]

In the dried membrane, the ionomer peak disappears, but the peak located in the wet membrane at q = 5.2 nm^{-1} remains, though slightly shifted to higher q, 6.3 nm^{-1} (see Figure 7). The values of the spacing corresponding to these peaks are 1.18 and 1.14 nm for the wet and dried membranes, respectively. These peaks reflect the fact that some kind of order developed in the dry membrane does not disappear in the wet membrane. The presence of mesogenic groups in the non-sulfonated imide

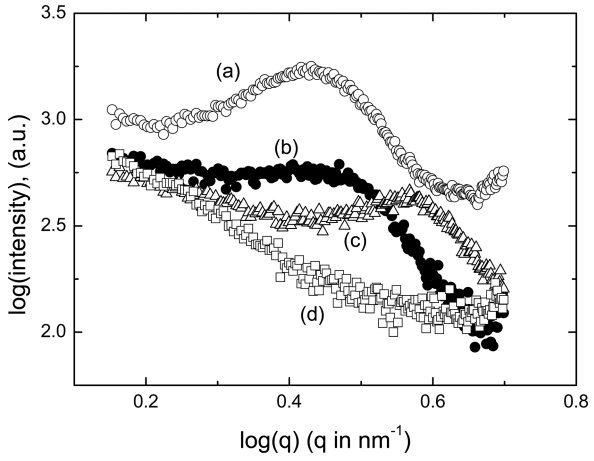

Figure 10. Variation of the ionomer peak with the hydration of the membrane. The values of λ at the beginning and at the end of the experiments were (a) 26.5 and unchecked, (b) 26.5 and 23.0, (c) 15.8 and 6.9, and (d) 3.5 and 1.9.

residues suggests that that peak may arise from bidimensional order developed in the hydrophobic regions of the membrane. That order presumably diminishes the swelling properties of the membranes, thus improving their mechanical stability. In the range $12.5° < 2\theta < 27.5°$, two highly overlapped weak peaks appear in the diffractograms of the dry membrane centered in the vicinity of 10.7 and 16.5 nm^{-1}. The presence of water in the membrane not only shifts the peaks to higher q but also partially deconvolves the peaks, giving rise to small peaks centered at 11.7 nm^{-1} followed by a relatively strong wide peak at 18.3 nm^{-1}. The spacing associated with this latter peak, 0.34 nm, suggests that it may be caused by naphthyl···naphthyl or phenyl···phenyl interactions favored by the presence of water in the membranes.

In the case of the fully hydrated membrane, the distance explored by the Li^+ in the conformational phase space in the MD simulations is slightly lower than 1 nm, a distance comparatively much lower than that explored in the ^7Li PFG-NMR experiments, which is on the order of micrometers. It is surprising that, in spite of the great differences of space explored by the two techniques, the values of the diffusion coefficients obtained are in rather good agreement for the membranes with higher water content. A large discrepancy between the values of the diffusion coefficients is observed at medium and low concentrations of water owing, most likely, to the fact that steady state conditions are not reached in the MD simulations. Although the simulated values of the diffusion of water in the membranes are somewhat higher than those measured by NMR, it is surprising that the observed dependence with the water content is similar. In fact, a vertical shift of the curves that describe log D vs λ for both techniques makes them roughly superpose.

The ratio between the tracer diffusivity and the tracer conductivity, denoted the Haven ratio H_R $(=D(^7Li)/D_\sigma)$, is normally less than 1 for most inorganic ionic systems.[1,2] Although a general theory of H_R is not yet available, this quantity for a hopping model of ionic conduction could be considered as the ratio of the tracer correlation factor f and the physical correlation factor f_{AA}, i.e., $H_R = f/f_{AA}$.[43,44] If collective correlations can be considered negligible, $H_R = f$. However, for a collective mechanism,the displacement of the tracer differs from that of the charge and the Haven ratio can be written as $H_R = fd^2/f_{AA}d_q^2$, where d and d_q are, respectively, the jump distances of the tracer and of the charge carrier (ref 1; Chapter 11, p 185). For high conducting membranes in the acidic form, such as Nafion, the transport process of the charge (H^+) is governed by the Grotthuss mechanism. ^1H PFG-NMR spectroscopy averages the trajectories of the rapid protons and the slow hydrogen atoms of water, and as a result, $H_R < 1$.[11] This fact has also been observed in studies of proton diffusion in this type of naphthalenic copolyimide-based membranes.[16] However, for membranes in which proton transport is of vehicular type, the Haven ratio approaches the unit and even can be higher.[17] The Haven ratio for lithium cation transport in the fully hydrated copolyimide membrane used in this study is 2.8. Since the charge carrier and the trace atom in the membranes used in this study is the same, the Haven ratio should be close to the unit, unless some lithium cations form some sort of ionic pairs which do not contribute to the conductivity. However, this possibility is unlikely because mobile co-ions that could intervene in ion-pair formation are excluded from the membrane. The ^{23}Na NMR spectra of polynorbornene based membranes functionalized with sulfonated dicarboxiimide side groups in the sodium form reveal the presence of isolated sodium ions together with sodium clusters in the membranes.[17] If that is the case in the membranes used in this study, and only the isolated lithium ions intervene in the charge transport, the concentration of ions would be smaller than that of fixed ionic groups in the membrane. Then, the value of D_σ obtained by eq 5 would be underestimated and as a result the magnitude of H_R overestimated. However, ^7Li and ^6Li NMR spectra do not provide any evidence of isolated lithium ions. Another way of explaining values of H_R above the unit is to postulate the presence of dead-end channels in the hydrophilic domains that decrease the ionic conductivity. Actually, although the NMR experiments average trajectories that extend over a relatively large space across the membrane, the values of the diffusion coefficients thus obtained are not so adversely affected by the presence of dead-end channels in the hydrophilic domains as the conductivity is. Notice that the thickness of the membranes lies in the vicinity of 50 μm, over 13 times the length of the NMR trajectories (3.7 μm for diffusion time of 60 ms). Haven ratios much higher than unit have also been reported for proton transport in imidazole based anhydrous membranes[45] and anhydrous ionomers.[46,47]

CONCLUSIONS

WAXS diffractograms of the hydrated membranes described in this work exhibit at low angles an ionomer peak located at q = 2.66 nm^{-1}, shifted to high q as the water content in the membranes decreases. The size of the segregated hydrophilic domains of the fully hydrated membrane is only 8% of that exhibited by block copolyimide membranes, and as a result, the conductivity of the fully hydrated membranes described in this work is about 10 times lower than that reported for block copolyimide membranes with similar ion-exchange capacity.

The WAXS diffractograms of the dry membranes do not present the ionomer peak observed in the wet membranes. However, the diffractogram of the dry membranes presents a peak at q = 6.3 nm^{-1} that is shifted to 5.2 nm^{-1} in the case of the fully hydrated membrane. The order reflected by this peak presumably confers mechanical stability to the membranes.

The diffusion coefficients of the lithium cation, obtained as a function of the water content of the membranes using ^7Li PFG-NMR techniques, are higher than those estimated from

conductivity utilizing Nernst–Planck type equations. Taking into account that the NMR technique averages over trajectories on the order of 3.5 μm and the thickness of the membranes lies in the vicinity of 50 μm, the discrepancy between the results obtained by the two techniques could be attributed to the existence of dead-end hydrophilic channels which do not contribute to the conductivity.

The results obtained for the diffusion coefficient of lithium cations in moderately high and fully hydrated membranes, computed using MD simulation techniques, agree with those measured by ^{7}Li PFG-NMR. This is a surprising result taking into account that the MD simulations only explore very short trajectories, in comparison with those explored by NMR. However, for medium and low concentrations, the time involved in the simulation is prohibitively long, thus impeding reaching steady state conditions using full molecular dynamics. As a result, the diffusion coefficients are overestimated.

The sizes of the first and second shells surrounding lithium cations and sulfonate anions are computed. The hydration numbers for Li^+ in the membranes with high water content come closer to those found for this cation in concentrated free dilute solutions.

ASSOCIATED CONTENT

Figures showing IR spectra, Nyquist and Bode plots, NMR spectra, thermogravimetric curve, trajectories represented by mean-square displacements of Li^+ and $O(H_2O)$, correlation distance functions, and the extended conformation of the sulfonated structural unit of the membranes. This material is available free of charge via the Internet at http://pubs.acs.org.

AUTHOR INFORMATION

The authors declare no competing financial interest.

ACKNOWLEDGMENTS

The authors acknowledge financial support provided by the DGICYT (Dirección General de Investigación Científica y Tecnológica) through Grant MAT2011-29174-C02-02.

REFERENCES

(1) Mehrer, H. *Diffusion in Solids*; Springer: Berlin, 2007.
(2) Dyre, J. C.; Maass, P.; Roling, B.; Sidebottom, D. L. *Rep. Prog. Phys.* **2009**, *72*, 046501 (and references therein).
(3) Capaccioli, S.; Lucchesi, M.; Rolla, P. A.; Ruggeri, G. *J. Phys.: Condens. Matter* **1998**, *10*, 5595.
(4) Krause, C.; Sangoro, J. R.; Iacob, C.; Kremer, F. *J. Phys. Chem. B* **2010**, *114*, 382.
(5) Carsi, M.; Sanchis, M. J.; Díaz-Calleja, R.; Riande, E; Nugent, M. J. D. *Macromolecules* **2012**, *45*, 3571.
(6) Sanchis, M. J.; Carsi, M.; Ortiz-Serna, P.; Díaz-Calleja, R.; Riande, E.; Alegría, L.; Gargallo, L.; Radic, D. *Macromolecules* **2010**, *115*, 5730.
(7) Jonscher, A. K. *Nature (London)* **1977**, *267*, 573.
(8) Burns, A.; Krysiccos, G. D.; Tombari, E.; Cole, R. H.; Risen, W. M. *Phys. Chem. Glasses* **1989**, *30*, 264.
(9) Paddison, S. J. *Annu. Rev. Mater. Res.* **2003**, *33*, 289.
(10) Maréchal, M.; Souquet, J. –L.; Gindet, J.; Sanchez, J.-Y. *Electrochem. Commun.* **2007**, *9*, 1023.
(11) Zawodzinski, T. A.; Neeman, M.; Sillerud, L. O.; Gottesfeld, S. *J. Phys. Chem.* **1991**, *95*, 6040.
(12) Jayakody, J. R. P.; Stallworth, P. E.; Mananga, E. S.; Farrington-Zapata, J.; Greenbaum, S. G. *J. Phys. Chem. B* **2004**, *108*, 4260.
(13) Roy, A.; Hickner, M. A.; Yu, X.; Li, Y.; Glass, T. E.; McGrath, J. E. *J. Polym. Sci., Part B: Polym. Phys.* **2006**, *44*, 2226.
(14) Zhang, J.; Giotto, V.; Wen, W.-Y.; Jones, A. A. *J. Membr. Sci.* **2006**, *269*, 118.
(15) Guo, X.; Zhai, F.; Fang, J.; Laguna, M. F.; López-González, M.; Riande, E. *J. Phys. Chem. B* **2007**, *111*, 13694.
(16) Garrido, L.; Pozuelo, J.; López-González, M.; Fang, J.; Riande, E. *Macromolecules* **2009**, *42*, 6572.
(17) Garrido, L.; López-González, M.; Tlenkopatchev, M.; Riande, E. *J. Membr. Sci.* **2011**, *380*, 199.
(18) Paddison, S. J.; Paul, R.; Kreuer, K. D. *Phys. Chem. Chem. Phys.* **2002**, *4*, 1151.
(19) Kreuer, K. -D.; Padison, S. J.; Spohr, E.; Schuster, M. *Chem. Rev.* **2004**, *104*, 46379.
(20) MacCallum, J. R., Vincent, C. A., Eds. *Polymer Electrolyte Reviews*; Elsevier: New York, 1987.
(21) Stephan, A. M. *Eur. Polym. J.* **2006**, *42*, 21.
(22) Golodnitsky, D.; Livshits, E.; Kovarsky, R.; Peled, E.; Chung, S. H.; Suarez, S.; Greebaum, S. G. *Electrochem. Solid-State Lett.* **2004**, *7*, A412.
(23) Page, K. A., Soles, Ch. L., Runt, J., Eds. *Polymers for Energy Storage and Delivery*; ACS Symposium Series 1096; Oxford University Press: Washington, DC, 2012.
(24) Samec, Z.; Trojánek, A.; Sameová, E. *J. Phys. Chem.* **1994**, *98*, 6352.
(25) Stenina, I. A.; Sistat, Ph.; Rebrov, A. I.; Pourcelly, G.; Yoroslavtsev, A. B. *Desalination* **2004**, *170*, 49.
(26) Volkov, V. I.; Pavlov, A. A.; Sanginov, E. A. *Solid State Ionics* **2011**, *188*, 124.
(27) Kreuer, K.-D. *J. Membr. Sci.* **2001**, *185*, 29.
(28) Watari, T.; Fang, J.; Tanaka, K.; Kita, H.; Okamoto, K.; Hirano, T. *J. Membr. Sci.* **2004**, *230*, 111.
(29) Stejskal, E. O.; Tanner, J. E. *J. Chem. Phys.* **1965**, *42*, 288.
(30) Garrido, L.; López-González, M.; Saiz, E.; Riande, E. *J. Phys. Chem. B* **2008**, *112*, 4253.
(31) Barsoukov, E., Macdonald, J. R., Eds. *Impedance Spectroscopy: Theory, Experiments and Applications*, 2nd ed.; Wiley: Hoboken, NJ, 2005; Chapter 2.
(32) Strictly speaking, drag of water by effect of the moving ions or electro-osmotic effect may also contribute to the conductivity in such a way that σ_{Li^+} in eq 5 should be replaced by $\sigma_{Li^+} - F\overline{u}_0X$, where X is the ion-exchange capacity of the membrane, $\overline{u}_0$ is the liquid mobility in the pores of the membrane, and F is Faraday's constant. However, for membranes with low electroosmosis, this correction can be considered negligible.
(33) Baron, M.; Kowalewski, V. J. *J. Phys. Chem. A* **2006**, *110*, 7122.
(34) Materials Studio Accelrys Inc., San Diego, CA [Accelrys Inc, San Diego, CA (Materials Studio 3.2, VISUALIZER, AMORPHOUS CELL and FORCITE modules)].
(35) Du, H.; Rosaiah, J. C.; Miller, J. D. *J. Phys. Chem. B* **2007**, *111*, 209.
(36) Materials Studio 3.2, VISUALIZER, AMORPHOUS CELL and FORCITE modules.
(37) Koneshan, S.; Rasaiah, J. C.; Lynden-Bell, R. M.; Lee, S. H. *J. Phys. Chem. B* **1998**, *102*, 4193.
(38) Garrido, L.; López-González, M.; Tlenlopatchev, M.; Riande, E. *J. Membr. Sci.* **2011**, *380*, 199.
(39) Yamagami, M.; Wakita, H.; Yamaguchi, T. *J. Chem. Phys.* **1995**, *103*, 8174.
(40) Schmidt-Rohr, K.; Cheng, Q. *Nat. Mater.* **2008**, *7*, 75 (and references therein).
(41) Essafi, W.; Gebel, G.; Mercier, R. *Macromolecules* **2004**, *37*, 1431.
(42) Geiculescu, A. C.; Rack, H. J. *J. Non-Cryst. Solids* **2002**, *306*, 30.
(43) Murch, G. E. Diffusion Kinetics in Solids. In *Phase Transformations in Materials*; Kostorz, G., Ed.; Wiley-VCh Verlag GmbH: Weiheim, Germany, 2001; Chapter 3.
(44) Murch, G. E. *Solid State Ionics* **1982**, *7*, 177.
(45) Scharfenberger, G.; Meyer, W. H.; Wegner, G.; Schuster, M.; Kreuer, K.-D.; Maier, J. *Fuel Cells* **2006**, *06*, 237.
(46) Herath, M. B.; Creager, S. E.; Kitaygorodsky, A.; DesMarteau, D. D. *J. Phys. Chem. B* **2010**, *114*, 14972.
(47) Herath, M. B.; Creager, S. E.; Kitaygorodsky, A.; DesMarteau, D. D. *ChemPhysChem* **2010**, *11*, 2871.